

# The behaviour of cationic NanoFibrillar Cellulose in aqueous media

Anna Olszewska · Paula Eronen · Leena-Sisko Johansson ·  
Jani-Markus Malho · Mikael Ankerfors · Tom Lindström ·  
Janne Ruokolainen · Janne Laine · Monika Österberg

Received: 19 April 2011 / Accepted: 5 July 2011 / Published online: 16 July 2011  
© Springer Science+Business Media B.V. 2011

**Abstract** This paper deals, with cationically modified NanoFibrillar Cellulose (cat NFC), obtained by reacting a dissolving pulp with 2,3-epoxypropyl trimethylammonium chloride (EPTMAC). The cat NFC was thoroughly characterized in terms of morphology and physical properties. The dimensions of individual cellulose nanofibrils were determined by atomic force microscopy (AFM) imaging in water and in air. Fibrils as thin as 0.8–1.2 nm were observed in water. The fibril diameter changed upon drying and the average size was further quantified by image analysis. The experiments showed the importance of characterizing nanocellulosic materials in situ before drying. The fibril size in air was confirmed by cryogenic transmission electron microscopy (cryo-TEM), and it

was found to be 2.6–3.0 nm. Smooth ultrathin films of cationic NFC were prepared by spincoating on silica substrates. The effect of electrolyte concentration and pH on swelling of the cationic NFC film was studied using a quartz crystal microbalance with dissipation. The results showed that at pH = 8 the cat NFC film was insensitive to electrolyte changes while at pH = 4.5, the water content of the film decreased with increasing ionic strength. The electrophoretic mobility measurements showed a cationic zeta potential for the cat NFC that decreased at increasing pH, verifying the swelling behaviour.

**Keywords** NanoFibrillar Cellulose · MFC · AFM · Fibril dimensions · Swelling · QCM-D

---

A. Olszewska (✉) · P. Eronen · L.-S. Johansson ·  
J. Laine · M. Österberg (✉)  
Department of Forest Products Technology, School of  
Chemical Technology, Aalto University, P.O. Box 16300,  
00076 Aalto, Finland  
e-mail: anna.olszewska@aalto.fi

M. Österberg  
e-mail: monika.osterberg@aalto.fi

J.-M. Malho · J. Ruokolainen  
Department of Applied Physics, School of Science, Aalto  
University, P.O. Box 15100, Puumiehenkuja 2,  
00076 Espoo, Finland

M. Ankerfors · T. Lindström  
INNVENTIA, AB Box 5604, Drottning Kristinas väg 61,  
114 86 Stockholm, Sweden

## Introduction

The properties of cellulose micro- and nanofibrils differ greatly from the properties of wood pulp fibres mainly because of the large specific surface area and high aspect ratio of the fibrils. The micro and nano scale fibrils have arrived to the public attention mostly due to their great mechanical properties combined with low weight, renewability and biodegradability (Siró and Plackett 2010). Another advantage of NanoFibrillar Cellulose (NFC) is that their production does not interfere with the food chain; therefore they can be considered as socially

sustainable raw materials. So far the unmodified (Pääkkö et al. 2007) and anionically modified nanofibrils (Saito et al. 2006, 2007; Wågberg et al. 1987, 2008) have gained most attention in the literature. The morphology, crystallinity, and surface interaction of ultrathin films made from unmodified and anionic NFC have been thoroughly studied (Ahola et al. 2008a, b; Aulin et al. 2009). In addition, the layer by layer assembly of anionic NFC together with different cationic polyelectrolytes have been investigated (Wågberg et al. 2008; Decher and Schlenoff 2003; Salmi et al. 2009). Also, the rheological behaviour and mechanical properties of unmodified NFC (Pääkkö et al. 2007), TEMPO oxidized NFC (Iwamoto et al. 2009) and bacterial-cellulose (Yano et al. 2005) were reported before. In pulp and paper applications, anionic NFC has been shown to have potential as a paper strength additive, although it has to be fixed to fibres using cationic polyelectrolytes for optimum performance and to reduce dewatering problems (Ahola et al. 2008a, b; Taipale et al. 2010).

It is known that nanocellulose fibrils possess intrinsically superior mechanical properties, such as high Young modulus of up to 135 GPa, and a high strength in the range of a few GPa's (Iwamoto et al. 2009; Yano et al. 2005; Sakurada et al. 1962), which suggests them to be excellent reinforcement agents in bio-based nanocomposites. These nano-scaled highly crystalline fibrils, which are made by breaking down the hierarchical cellulose fibers, are long enough for good stress transfer in a polymer matrix, hence improving the mechanical properties of the composites. The use of NFC in nanocomposites was recently reviewed by Eichhorn et al. (2010). Lately a new concept for the utilization of NFC in biomimetic nanocomposites, where the synergic effect of the components beyond the simple rule of mixture was observed, has also been introduced (Wang et al. 2011).

Cationic NFC could have potential both in high end applications as nanocomposites and high volume applications in the paper industry. It is known that cationic materials often are biocidal (Gilbert and Moore 2005) therefore cationic NFC could improve mechanical properties of composites just as the anionic NFC but additionally give the material antibacterial properties. Cellulosic fibres for paper manufacture are anionic; hence cationic NFC may replace cationic polyelectrolytes as efficient strength additives. However, as yet, cationic NFC has not

been either thoroughly characterized or utilized in applications except for one recent publication by Aulin et al. (2010). The authors used cationic NFC to build all cellulosic multilayers from anionic and cationic NFC by the layer by layer (LbL) technique. Yet, to fully utilize the potential of cationic NFC it is necessary to understand the colloidal and physical properties of the fibrils as well as what influence, the cationic modification has on the size of the fibrils.

The fibril size is of great importance when it comes to mechanical properties of materials made from NFC (Dufresne et al. 2003). In fibres the high cohesion of fibrils obstructs cell wall delamination but by applying high mechanical shear-forces and chemical (oxidation/charging) or enzymatic pre-treatments (Pääkkö et al. 2007; Wågberg et al. 1987, 2008), it is possible to disintegrate the fibres. The nanofibril diameter distribution is strongly influenced by both the manufacturing process as well as the cellulose source. Moreover, the presence of non-cellulosic materials such as hemicellulose and pectin influences cell wall cohesion and can make delamination easier to achieve (Virtanen et al. 2008; Iwamoto et al. 2008). Chemical modification prior to disintegration increases the fibrillation efficiency and thinner fibrils can be obtained. Previous investigations have shown that increasing the charge of fibrils by either carboxymethylation (Wågberg et al. 1987, 2008), or TEMPO-mediated oxidation results in a smaller fibril size and smoother and denser films (Ahola et al. 2008a, b; Aulin et al. 2009; Saito et al. 2007). The smallest lateral dimension reported for unmodified NFC fibrils disintegrated from wood, is around 5 nm (Pääkkö et al. 2007) i.e. in the order of the size of the elementary fibrils. More often the fibrils occur as intertwined fibril bundles (fibril aggregates) with widths around 20–25 nm (Hult et al. 2001; Meshitsuka and Isogai 1996; Bardage et al. 2004). Recently, individual fibrils in the range of 3–4 nm (Saito et al. 2007) and 2.5–4 nm (Johnson et al. 2009) have been observed for TEMPO-oxidized NFC, that correlate well with the dimensions of elementary cellulose fibrils from Norway Spruce,  $2.5 \pm 0.2$  nm (Jakob et al. 1995). Cryogenic transmission electron microscopy (cryo-TEM) has previously been used to image non-aggregated NanoFibrillar Cellulose (Saito et al. 2007). However, another possible method that has not yet been extensively used for characterization of cellulose in never dried state, except for the early studies on crystalline structure of cellulose I

microcrystals from Valonia (Baker et al. 1997) is liquid state AFM.

In the present study AFM in both water and air was used to characterize the dimensions of the cationic NFC in some detail. The results were compared to cryo-TEM images to emphasize the effect of the media on the observed dimensions. Since most applications of the cationic NFC are expected to be in an aqueous environment, the swelling behaviour of ultrathin films of cationic NFC in various pHs and electrolyte concentrations was studied using the quartz crystal microbalance with dissipation monitoring (QCM-D).

## Experimental section

### Preparation of NFC dispersion

Cellulose nanofibrils were liberated from bleached sulphite dissolving pulp (Trade name: Dissolving Plus, Domsjö Fabriker, Domsjö, Sweden) by using a cationization pre-treatment followed by a high-pressure homogenization. The Domsjö pulp has a hemi-cellulose content of 4.5%, measured as the solubility in 18% NaOH. The anionic charge density of the pulp was determined to be 28  $\mu\text{eq/g}$  by conductometric titration (Katz et al. 1984). The cationization of the cellulose was done by reaction of the dissolving pulp with N-(2-3-epoxypropyl) trimethylammonium chloride (EPTMAC) (Sigma, Aldrich, Germany). To a 50 g of a 20% aqueous dissolving pulp dispersion 5 g EPTMAC was added together with 0.8 g NaOH dissolved in 0.8 g water. The dispersion was diluted with 100 mL isopropanol and was allowed to react at 50 °C for 2 h after which the cationic pulp was washed with an excess of deionized water. The cationic pulp was then homogenized to create the cationic NFC dispersion (Aulin et al. 2010). The cationic charge density was determined to be 354  $\mu\text{eq/g}$  (degree of substitution (D.S.) = 0.08) by N-analysis (Chemiluminescence, Antek 7000, Antek Instruments Inc. USA). The homogenization was done using a high-pressure fluidizer (Microfluidizer M-110EH, Microfluidics Corp., Newton MA) at Innventia, Stockholm, Sweden.

### NFC film preparation

Silica wafers (Okmetic Oy, Finland) and Muscovite mica were used as substrates for the NFC films for

high-resolution AFM imaging and silica coated QCM-D crystals (QSX 303, Västra Frölunda, Sweden) were used for QCM-D experiments. The silica substrates were, washed before used in 10% NaOH solution for 20 s and rinsed with Millipore water, and finally dried with nitrogen gas. Prior to use they were UV/ozone treated for 15 min rinsed with water and finally dried with nitrogen.

The nanofibril dispersions were diluted to 1.67 g/L concentration, ultrasonicated using a micro tip (Branson Digital Sonifire s-4500, Branson corp., Danburg, CT) for 10 min at 25% amplitude and centrifuged at 10,000g for 45 min. The clear supernatant (1.5 g/L) was used for spin coating. The cellulose model surfaces were prepared by spin coating aqueous nanofibril dispersions onto a freshly cleaned silica substrate. The fibril dispersion was spread on the substrate and the sample was spinned at 3,000 rpm for 45 s. After spin coating the surfaces were rinsed with water, gently dried with nitrogen gas, and heat-treated in an oven at 80 °C for 15 min (Ahola et al. 2008a, b).

### Mobility measurements (Zeta potential, DELSA)

The zeta potential of the nanofibril aqueous dispersion was measured using a Doppler Electrophoretic Light Scattering Analyzer (DELSA) 440 From Coulter Electronic, USA. The NFC dispersion was diluted to 1 g/L, dispersed by ultrasonication and centrifuged at 10,000g. The mobility of the supernatant was determined at a constant electrolyte concentration (10 mM NaCl). The pH of the samples was adjusted with small amounts of HCl or NaOH.

### Atomic force microscope imaging (in air and water) (AFM)

For the characterization of NFC fibril dimensions and surface coverage, roughness, morphology and thickness of the NFC films, atomic force microscopy (AFM) imaging in air and water was applied. The Nanoscope IIIa multimode scanning probe microscope (Digital Instruments Inc., Santa Barbara, CA) operating in tapping mode was used. The images in air were performed using silicon cantilevers (NSC15/AIBS, MicroMasch, Tallinn Estonia) with a driving frequency around 300–360 kHz. The radius of the tip according to the manufacturer was less than 10 nm.

The size of the images was  $1\ \mu\text{m}^2$  or  $25\ \mu\text{m}^2$ , and the images were scanned on at least three different areas of the sample. Scratching the films with a needle and scanning over the scratch at several points determined the thickness of the films. For the imaging of never dried nanofibril samples, the fibril dispersion was adsorbed on mica. The dispersion medium was then changed to fresh water and the samples were scanned in tapping mode in water. Soft silicon cantilever (Non-contact ultra-sharp silicon cantilevers NSCS12, NT-MDT) was used with a driving frequency between 7 and 11 kHz. The size of the images was  $1\ \mu\text{m}^2$ . No other image processing except flattening was applied. All quantitative data was extracted from the height images. Image analysis was performed using NanoScope software (version V6.13R1(R) Digital Instruments, Inc.). The size of the individual fibrils was measured with help of Scanning Probe Image Processor (SPIP) software (version 4.5.3, Image Metrology, Lyngby, Denmark).

To determine the size distribution of fibrils in the AFM images a method developed at Center for Image Analysis in Uppsala, which is based on the watershed algorithm was used (Fahlen and Salmen 2003; Wählby et al. 2001). For each image, the software detects the different fibrils. Since the fibrils were in a network the visible fibrils are very short. The software calculates the longest and the shortest dimensions of the visible part of the fibrils in the AFM image. The shortest dimension corresponds to the fibril widths.

#### Cryogenic transmission electron microscopy (Cryo-TEM)

A Jeol JEM-3200 FSC microscope was used for the Cryo-TEM (Cryogenic Transmission Electron Microscopy) imaging to characterize the morphology and size of the fibrils. 200 mesh copper grids with holey carbon foil, Quantifoil R2/2, were treated with oxygen and hydrogen plasma (Gatan, Model 950 Advanced Plasma System) for 30 s, the target vacuum was 70 mTorr and the target power was 50 W,  $\text{O}_2$  gas flow was 27.5 sccm (standard cubic centimeter per minute) and the  $\text{H}_2$  gas flow was 6.4 sccm prior to sample preparation. The plasma treated grid was placed into a FEI Vitrobot having room temperature and 100% relative humidity. Three microlitre of sample solution was applied onto the grid and the excess of the dispersion was removed by a blotting paper for 2 s

(Whatman filter paper). 1:1 liquid propane-ethane mixture cooled to  $-180\ ^\circ\text{C}$  was used for sample vitrification. The vitrified sample was cryo-transferred into the microscope and continuously cooled during the imaging process at  $-188\ ^\circ\text{C}$ . Micrographs were recorded with a Gatan Ultrascan 4,000 camera operating microscope at bright field mode, at 300 kV acceleration voltage and with Omega type in-column energy filter set to 0–20 eV electron energy-loss range (zero-loss imaging).

#### X-ray photoelectron spectroscopy (XPS)

The surface chemical composition of the model surfaces was investigated using X-ray photoelectron spectroscopy (AXIS 165, Kratos Analytical, Shimadzu Group, Japan). Prior to the experiments, the samples were pre-evacuated overnight together with an in situ reference (100% cellulose) (Johansson and Campbell 2004). Throughout the experiment, monochromatic Al K ( $\alpha$ ) irradiation at 100 W was utilised. Elemental surface concentrations were determined from low-resolution wide scans using 1 eV step and 80 eV analyser pass energy, except for nitrogen. For quantification of very small nitrogen contents, regional N 1 s spectra were collected, using settings similar to the wide scans. The surface chemistry of carbon and oxygen were evaluated from high-resolution measurements of C 1 s and O 1 s regions, using 0.1 eV step and 20 eV analyser energy. The analysis area was around  $1\ \text{mm}^2$  and the analysis depth was less than 10 nm. No sample deterioration due to UHV or irradiation was observed, and according to the data from the in situ reference, experimental conditions remained satisfactory throughout the experiment. Due to the insulating nature of the samples, neutralisation with slow thermal electrons was utilised during the data acquisition, which is why the binding energies in regional spectra were charge corrected after the measurement, using aliphatic carbon compound of C 1 s signal at 285 eV as a reference (Beamson and Briggs 1992).

#### Sample preparation for Raman spectroscopy

Freestanding films were prepared from nanocellulose gels. The gel was first diluted to 0.1 w-% consistency with MilliQ—water, vigorously shaken and further homogenized with ultrasound microtip (Branson

Sonifier S-450 D, Danbury, USA) and bath (Sonorex DT 52H, Bandelin GmbH & Co. KG, Berlin, Germany) treatments. The aqueous fibril dispersions were cast over a plastic petri dish and allowed to dry in room temperature for several days. Small pieces were cut from the centre of the film (thickness 50  $\mu\text{m}$ ). The samples were analysed with Confocal Raman spectrometer (WITec alpha 300R, WITec GmbH, Ulm, Germany) in ambient room temperature. Raman spectra were collected from the dried nanocellulose films with a frequency doubled Nd:YAG green laser (wavelength 532.14 nm, power  $\sim 30$  mW) and Nikon 100 $\times$  (NA = 0.90) air objective. The grating of the spectrogram used was 600 grooves/mm and the optical fibre to collect the scattered photons had a diameter of 50  $\mu\text{m}$ . The excitation light was polarized horizontally in *x*-direction. A sensitive electron multiplying (EM) CDD camera (Andor Newton DU970-BV, Andor Technology plc, Belfast, UK) was used as detector. Integration time for individual spectra was 2 s, and 5 accumulations were collected from minimum 10 different sample positions. The spectra were only base-line subtracted using software provided with the instrument (WITec Project).

#### Quartz crystal microbalance with dissipation (QCMD)

The water uptake of nanofibril cellulose films was studied by means of a quartz crystal microbalance with dissipation (QCM-D) using the E4 instrument from Q-Sence AB, Västra Frölunda, Sweden. The E4 instrument has an axial flow chamber and allows simultaneous measurements of both frequency and dissipation changes (frictional losses due to viscoelastic properties of the adsorbed layer) at the fundamental resonance frequency, 5 MHz and its overtones 15, 25, 35, 45, 55, and 75 MHz. Right after starting the measurements the pump was turned into the low flow rate 0.1 mL/min. All experiments were repeated at least two times. For rigid, thin and homogeneous adsorbed films, the change in frequency,  $\Delta f$ , is proportional to the adsorbed mass per unit surface,  $\Delta m$ , according to the Sauerbrey equation (Sauerbrey 1959). However, in the case of thicker films, which show pronounced viscoelastic effects, the Sauerbrey equation is no longer valid. Johannsmann et al. (1992) presented a model, which allows

calculation of the true sensed mass for viscoelastic layers. That model has been used in this study to calculate the mass adsorption:

$$\hat{m} = m^0 \left( 1 + \hat{J}(f) \frac{\rho f^2 d^2}{3} \right) \quad (1)$$

The true sensed mass ( $m^0$ ) can be calculated by assuming that  $\hat{J}(f)$ , (which is the shear compliance), is independent of the frequency in the accessible frequency range. By plotting the equivalent mass against the square of the resonance frequency ( $f^2$ ), the true sensed mass is given as the intercept (Naderi and Claesson 2006).

## Results and discussion

### The nature of amphoteric NFC

The cationic nanofibrils were characterized in terms of morphology and their interactions with water. The charge was introduced by the aquatic reaction of dissolving pulp with N-(2,3 epoxypropyl) trimethylammonium chloride in the presence of a base. The quaternized amine is positively charged at all pH-values. The cationic charge density was determined to be 354  $\mu\text{eq/g}$  (degree of substitution (DS) = 0.08). The charged was determined for fibres; however unpublished data show that it doesn't change after fibres are disintegrated. The NFC, however, also possess some carboxyl groups originating mainly from the residual hemicelluloses in the pulp with a small amount attributable to cellulose oxidation during the pulping operation. The anionic charge was measured by conductometric titration to be 28  $\mu\text{eq/g}$ . These groups start to deprotonate at pHs above 2.5, meaning that the net charge of the cationic NFC is pH dependent. The zeta potential of the NFC was studied in order to confirm that the pH affects the net charge of the fibrils. In Fig. 1 the zeta potential as a function of pH for aqueous cationic NFC dispersions is shown. In the pH range studied (3–11) the nanofibrils are positive. However, the net charge is clearly pH dependent. The highest positive potential is observed at pH 3 and the z-potential decreases with increasing pH. This is as expected due to the increasing amount of dissociated carboxyl groups on the NFC surface as the pH increases.



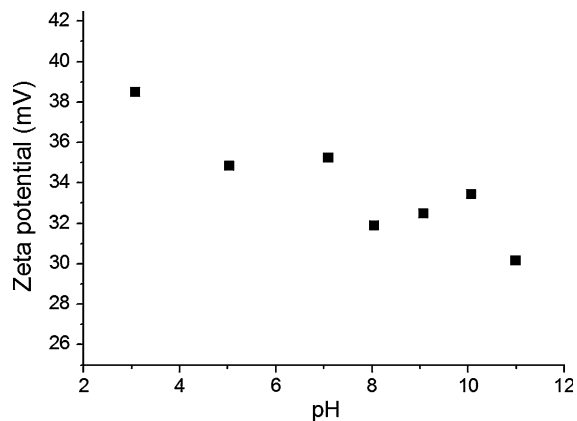


**Fig. 1** The zeta potential of the cationic NFC dispersion as a function of pH

### Nanofibril morphology in the never dried state and the effect of drying

Figure 2 summarizes the size characterization of cationic NFC fibrils by using AFM in water and air. To obtain a detailed picture of the fibril dimensions both average widths distribution determined by image analysis (Fig. 2c, h) as well as high-resolution inspection of the height of individual fibrils (Fig. 2b, g) was performed. In summary the observed fibril width was very small, in average 4 nm and even around 1 nm for the finest fibrils observed in water showing that the cationization pre-treatment is very efficient in liberating the fibrils and the fibril dimensions suggest that un-aggregated microfibrils are

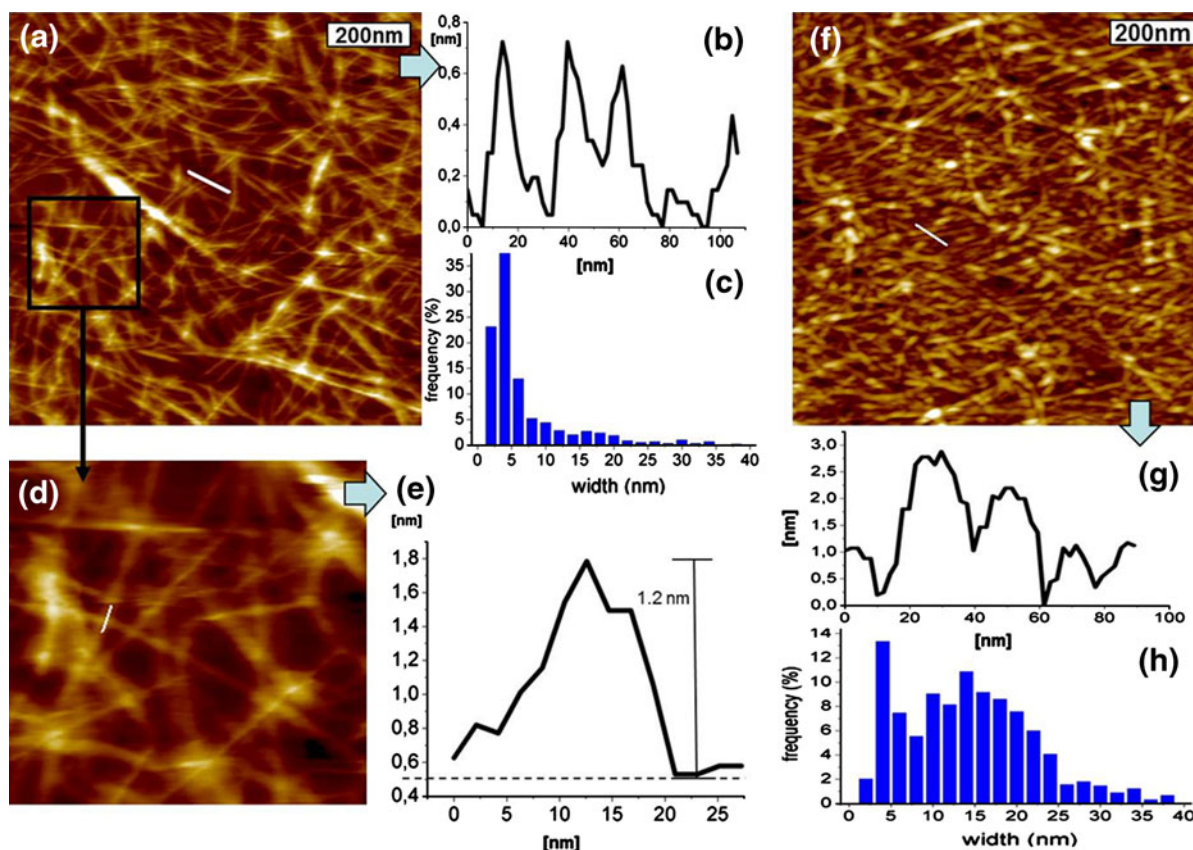


**Fig. 2** AFM height image of never dried cationic nanofibrils adsorbed on mica from an aqueous dispersion, imaged in water (a). From the line scans it is observed that the height of the fibrils in water is around 0.8–1.2 nm (b). Size distribution analysis data (c) for never dried NFC imaged in liquid, are also presented. *Black square* (d) shows magnification from (a) and the height of the fibril aligned on top of another fibril (e). The

AFM height image of the same sample imaged in air after drying is presented in (f). A representative height profile for dried fibrils is presented in (g) and the average width based on image analysis for dried samples in (h). The scan size for both the never dried and dried film was  $1 \times 1 \mu\text{m}^2$ . The z-scale in the height images is 5 nm (a) and 8 nm (f) for images in water and in air respectively

obtained. It was found that the fibril width in aqueous media is smaller compared to the same fibrils after drying. Figure 2a presents an AFM height image of never dried cationic NFC fibrils adsorbed on mica. The fibril size estimated from the height of the fibrils directly attached to mica was found to be between 0.8 and 1.2 nm for the smallest non-aggregated fibrils. The height was used for the size evaluation since the diameter of features is overestimated due to the dimensions and geometry of the AFM tip (Wang and Chen 2007). To ensure that the observed thin dimensions are not artifacts the height of a fibril which was aligned on top of another fibril was also measured (see magnification in Fig. 2d and height profile Fig. 2e). We found that the size was around 1.2 nm, which still is surprisingly small compared to any previously reported sizes of cellulose nanofibrils (Wågberg et al. 2008; Saito et al. 2006). From Fig. 2a it is evident that the fibrils chosen for the line scans (Fig. 2b and e) are representative for the nonaggregated fibrils and many similar sized fibrils are found. The size distribution was also quantified using image analysis for the AFM image of cationic NFC in liquid. In this case the width of the fibrils was used for the analysis, which may overestimate the dimensions due to the dimensions and geometry of the AFM tip. 74% of the fibrils were 6 nm or less in width, the most frequent width being 4 nm (Fig. 2c). Theoretically the cellulose crystallite cross section could be from  $1.5 \times 2 \text{ nm}^2$  to maximum  $3 \times 5 \text{ nm}^2$  calculated on the basis of the model cellulose I $\beta$  crystal structure (Ding and Himmel 2006). It was also reported that ultrasonication could cause further disintegration of microfibrils leading to isolation of molecularly thin sub-microfibrillar structures (Li and Rennecker 2009). These authors postulated that the sonication breaks up the inter-sheet van der Waals bonding of the cellulose fibrils, thus, liberating smaller fibrils. However, a recent study by Gross and Chu (2010) shows that inter-sheet interactions, which involve C–H–O pseudo hydrogen bonding and van der Waals interactions appear to be the strongest, most stable interactions in the network. Although increasing the charge by e.g. carboxymethylation or TEMPO mediated oxidation (Wågberg et al. 2008; Saito et al. 2007) prior to disintegration facilitates smaller fibril size, the size of individual fibrils previously reported have been in the range of 2.5–4 nm, (Johnson et al. 2009) thus considerably

larger than observed here. The sonication, used to disperse the cationic fibrils prior to the film preparation could be one reason for the sub-microfibrillar structures. Nevertheless, the same sonication step has been used for unmodified and anionic NFC without breaking down the microfibrils (Ahola et al. 2008a, b).

Interestingly, the height of fibrils increases upon drying. Figure 2f shows the AFM image of the same cationic NFC film adsorbed on mica after drying. The size of fibrils estimated from height profile was in the range of 2.5–3 nm. The dimensions observed here correlate with the dimensions of elementary cellulose fibrils from Norway Spruce  $2.5 \pm 0.2 \text{ nm}$ , obtained using TEM, Small-angle X-ray Scattering and wide-angle X-ray scattering (Jakob et al. 1995). The increase in the size of fibrils during the transition from wet to dry stage could be caused by the aggregation, clustering of the fibrils as a consequence of the high density of hydroxyl groups on the surface of the fibrils (Zimmermann et al. 2004). However, aggregation of the already adsorbed fibrils that further would be perfectly aligned so that the fibrils appear thicker seems unlikely. The dimensions of NFC obtained by AFM imaging in air correlated well with the cryo-TEM images (Fig. 3). Cryo-TEM was performed on the well dispersed (sonicated and centrifuged) NFC dispersion, adsorbed on a copper grid followed by sample vitrification. Micrometer long cationic nanofibrils with a slight distribution of the diameter 2.6–3 nm were observed in the TEM micrographs. The image analysis for the dried samples (from AFM data) shows a wide distribution of the fibril width (Fig. 2g). It is clearly seen that the size of the fibrils has increased after drying the sample.

We can only speculate on the reason behind the discrepancy between fibril dimensions of never dried fibrils in aqueous media measured using AFM and cryogenically or air-dried fibrils measured by TEM and AFM respectively. Since chemically modified NFC has not been characterized by AFM imaging in wet state this phenomenon has not been observed before. Previously Ding and Himmel (2006) proposed that elementary fibril is a heterogeneous structure containing a crystalline core and layers of sub-crystalline/Para crystalline sheaths. Using solid state  $^{13}\text{C}$  NMR, the structural disorder of the surface chains was demonstrated (Vietor et al. 2002). It is

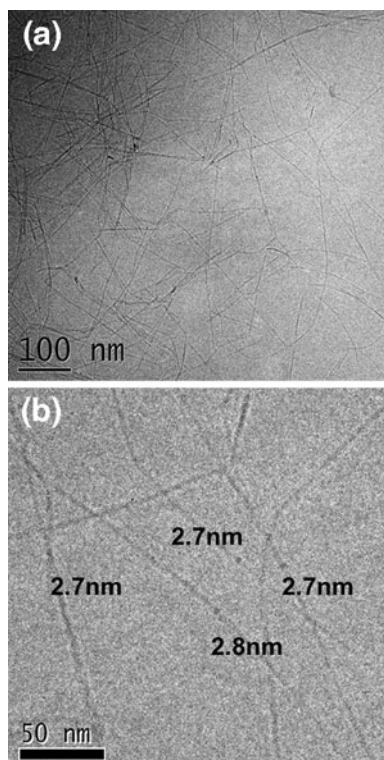


**Fig. 3** Cryo-TEM of the frozen 0.9 g/L NFC aqua solution after the cationization and homogenization processes showing a fibrillated network of nanoscale fibrils (a) and individual fibrils (b)

possible that for the cationic fibrils, a disordered outer layer on the fibril is present in the wet stage but reorganizes on the fibril core during drying. It has been previously shown that this kind of reorganization of cellulose molecules is possible in the case of fully dissolved cellulose. Langmuir–Blodgett films, which are made from fully dissolved cellulose (through the derivative trimethyl silylcellulose, TMSC) possess fibrillar film structure and a crystallinity around 60%, meaning that some reordering (recrystallization) has occurred during either deposition or drying step (Aulin et al. 2009). Analogously it is known that selective etherification of cellulose perturbs inter-chain interaction and leads to a significant disruption of the crystallinity of cellulose and hence increases its solubility (Kondo 1997). It is proposed that due to this modification the surface layer of the fibrils is partly dissolved creating a core shell type structure of the fibril. The inner part of the fibril is largely unaffected by the modification and

remains highly crystalline and rigid. However, the outer layer is in aqueous media diffuse and partly dissolved. This diffuse outer layer is supposedly not detectable by the AFM tip. Subsequently that leads to the false observation that the fibrils are smaller than the elementary fibril in the wet state. The tip scans only the rigid core of the fibril. However, when dried, the disordered layer can organize and possibly recrystallize on the core of the fibrils, and the fibrils appear thicker. Prior to cryo-TEM analysis the fibrils are frozen in the non-aggregated and swollen state. However, the dimensions observed using cryo-TEM are closer to the dimensions observed in air using AFM.

#### Characterization of spin-coated cationic NFC films

For better comparison with previous literature data the cellulose nanofibril films used for QCM-D studies were further characterized in air with respect to surface morphology, roughness and thickness. Figure 4a and b shows a fibrillar network structure, which has an average rms roughness of 0.97 nm. The roughness was determined from 25  $\mu\text{m}^2$  areas. Previously Ahola et al. (2008a) have examined films from anionic nanocellulose, where the rms roughness of highly charged; carboxymethylated cellulose and low charged unmodified anionic nanocellulose films were 2 nm and 4 nm respectively (Ahola et al. 2008a).

The very fine thickness of the cationic NFC and the good affinity of the fibrils directly to silica surfaces facilitate the formation of a very smooth film. The average thickness of cationic NFC films was 2 nm and 5 nm for monolayer and nine spin coated layers, respectively. The cationic NFC films were thinner than the anionic films characterized previously (Ahola et al. 2008a). According to the AFM images the cationic nanofibrils form a homogeneous network fully covering the substrate. Several 25  $\mu\text{m}^2$  areas were measured, and no open spots were detected.

XPS was used to characterize the chemical composition of the cationic nanofibril films, see Fig. 5. A clean  $\text{SiO}_2$  surface and a Whatman filter paper were used as references. In this experiment, films prepared by spin coating of one or nine layers of NFC were used. The appearance of the sharp C–O peak—typical for cellulose (Johansson and Campbell 2004) in the



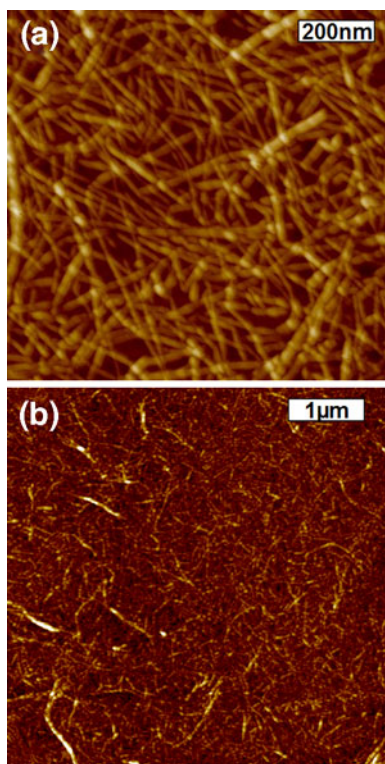


**Fig. 4** AFM height image of monolayer cationic nanofibril model films spin-coated on silica substrate image in air. The scan size is  $1\ \mu\text{m} \times 1\ \mu\text{m}$  (a) and  $5\ \mu\text{m} \times 5\ \mu\text{m}$  (b). No anchoring substance was used

carbon C 1 s high-resolution spectra (Fig. 5b) indicates that the silica surface is covered with NFC. The film, which consisted of only one spin coated layer, still had a quite a high silicon content (Fig. 5c). This is most likely due to the fibrillar structure of the very thin layer of NFC layer resulting in an open network. As expected, increasing the number of spin-coated layers increased the cellulose signal in XPS data, although some Si from the substrate was detectable in all spin-coated samples. However, after nine layers the Si signal had decreased to 12 at% and the inelastic spectral background tailing the silicon signals had increased (in relation to the respective silicon signals), indicating that the substrate was mainly covered (Johansson et al. 2004). Figure 5d depicts the nitrogen data obtained from XPS, trace measurements, which are of interest, since they indicate the degree of amine group substitution. The degree of cellulose substitution was calculated to be 0.06 for cationic films spin coated on silica (the value is calculated from the ratio N/Cellulose), which is lower

than the value obtained for a thick, unsupported film from the same material (0.14). Furthermore, the charge corrected binding energy for the nitrogen N 1 s peak was 403 eV, which is in good agreement with the published reference value for  $^+\text{N}(\text{CH}_3)_3$  (Beamson and Briggs 1992) (Fig. 5d).

The cationization of the fibrils was verified by using Raman micro spectroscopy. The Raman spectra measured from dried free-standing films of cationized NFC and anionic carboxymethylated NFC are shown in Fig. 6. The carboxymethylated fibrils were prepared according to the procedure describe elsewhere (Wågberg et al. 2008) and were used here for comparison. The characteristic Raman bands for cellulose I structure can be identified from both spectra, indicated with stars in Fig. 6. A conversion to cellulose II would decrease the relative intensity of the band at  $1,120\ \text{cm}^{-1}$  and lower degree of crystallinity leads to broader less defined peaks. This confirms that the surface modification of the fibrils do not affect the cellulose polymorphy. The orientation of the fibrils relative to the horizontal polarization of the incident light strongly affects the relative intensities at the band positions  $1,095\ \text{cm}^{-1}$  (COC glycosidic linkage) and  $2,895\ \text{cm}^{-1}$  (CH stretching), but does not affect the clearly identified bandwidth positions (Wiley and Atalla 1987; Eronen et al. 2009). In addition, from the cationized cellulose the substituted trimethyl ammonium group can be observed. Distinct new bands at positions 761 and  $3,030\ \text{cm}^{-1}$  are caused by symmetric stretching of the  $(\text{CH}_3)_3\text{-N}^+$  and  $\text{CH}_3$  antisymmetric stretching, respectively (Phillips et al. 1999; Pigorsch 2009). Thus the Raman microspectroscopy clearly confirmed the cationic modification of the cellulose fibrils.

#### Effect of pH on water binding capacity of cationic NanoFibrillar film

The effect of electrolyte concentration on the swelling of cationic cellulose nanofibrils film was studied at pH 8 and 4.5. The swelling of cellulosic fibril network can be compared to the swelling of poly-electrolyte gels (Ahola et al. 2008a, b) and it is controlled by the charge density of cellulose, the ionic strength of the surrounding medium, the type of counter ions, and the degree of cross-linking (Flory 1953). By using the QCM-D technique it is possible

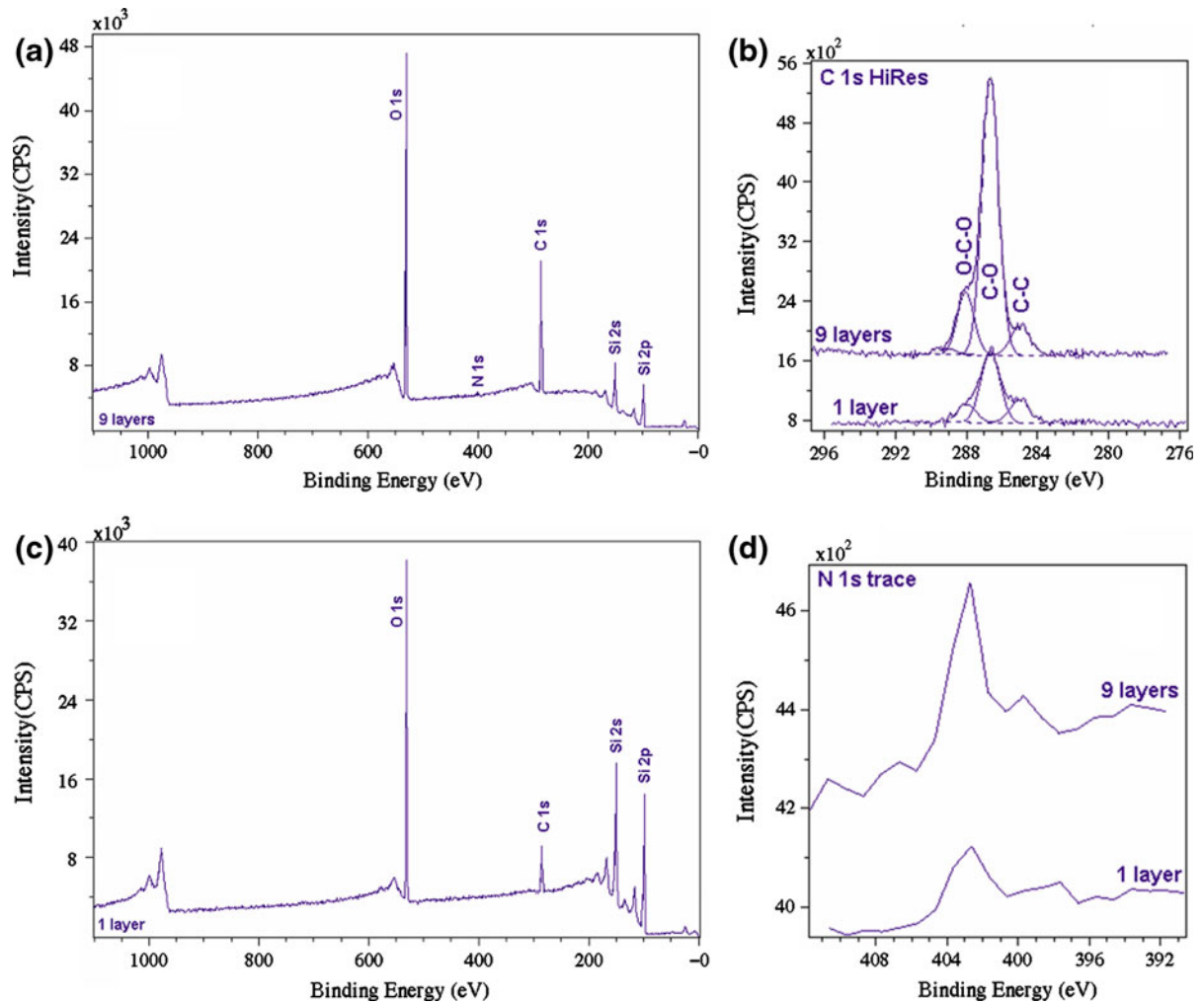


**Fig. 5** XPS wide scan spectra of 9 (a) and 1 spin coated layers (c) of cationic NFC films on silica substrate, and high resolution XPS spectrum of carbon 1 s (b) and low resolution XPS spectrum of nitrogen 1 s (d)

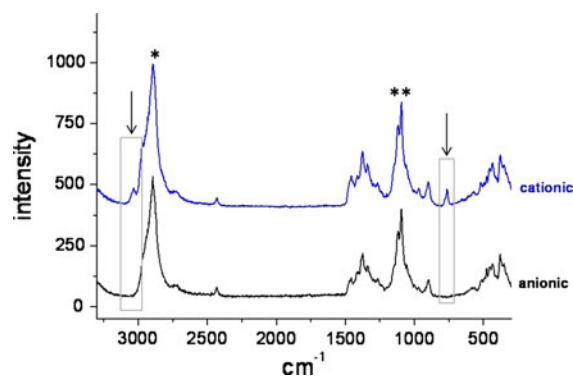


**Fig. 6** Raman spectra of carboxymethylated and cationic NFC. The arrows indicate the new bands emerging from cationic modification

to study the adsorption and swelling of cellulosic model surfaces in situ. This sensitive technique also allows the monitoring of the kinetics of such processes as well as the viscoelastic changes in the monitored cellulosic films during the measurements (Kontturi et al. 2006; Fält et al. 2003; Tammelin et al. 2006). Figure 7 shows the changes in frequency and dissipation at respective pH and at different concentrations of sodium chloride. First air was passed through the QCM-D chamber and when the baseline was stable at  $(t) = 5$  min, 1 mM buffer solution was added. The frequency change upon addition of the buffer for cationic NFC films at pH 8 ( $\text{NaHCO}_3$  buffer) and 4.5 ( $\text{NaAc}/\text{HAc}$  buffer) was  $-460$  and

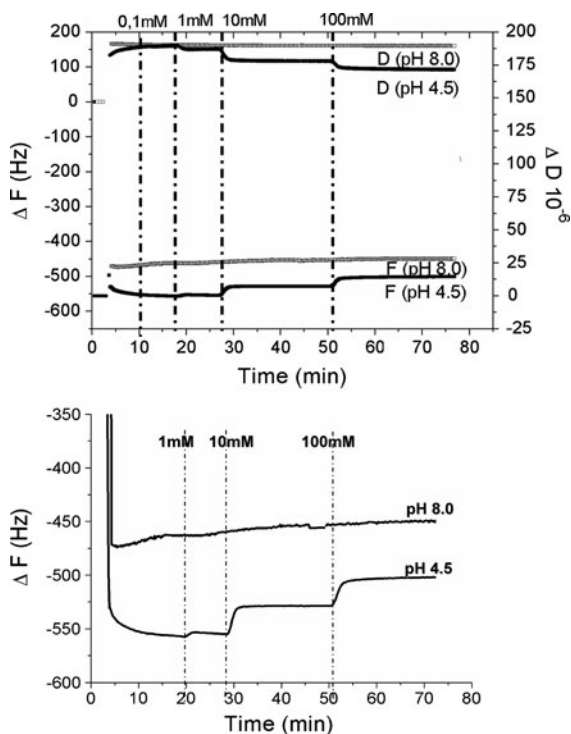


**Fig. 7** QCM-D data (3rd overtone) showing the effect of electrolyte concentration at different pH on the change in frequency and dissipation for cationic cellulose nanofibril films. The *lower graph* zooms into emphasis the effect of electrolyte concentration on the water content in the film

–550 Hz, respectively. We have previously determined the change in frequency caused by the bulk effect (i.e. viscosity difference between air and aqueous buffer) to be –386 Hz (for the third overtone) for silica crystals (Aulin et al. 2009). Most of the water uptake took place in this initial phase immediately after introducing the aqueous buffer solution. The cellulose surface continued to swell slowly at pH 4 while almost no further change was detectable at pH 8. There are mainly two reasons for the extensive swelling of the nanofibrillated cellulose film. Firstly, the high amount of accessible hydroxyl groups in the open network of nanofibrils and secondly the charged groups in cationic NFC. Due to the charged groups NFC behaves as a polyelectrolyte gel. The higher the charge of the NFC, the more water the film binds. An increase in the electrolyte concentration, on the other hand, is expected to decrease the water uptake due to a decreased electrostatic repulsion between the charged groups in the gel.

The water uptake for the cationic NFC film varied at different pH. At high pH-values (pH 8.0) where the carboxyl groups are deprotonated, they will lower the net cationic charge in the NanoFibrillar gel and, hence the water uptake will be lowered. Equation 1 was used to calculate the mass of water adsorbed in the film. The dry mass of the film was estimated by using the thickness (2 nm) and area (0.785 cm<sup>2</sup>) of the film and assuming that the density of cellulose is 1.592 g/cm<sup>3</sup> (Sugiyama et al. 1991; Mwaikambo and Ansell 2001). For all measured films the dry mass of cellulose was the same and the calculated value was 3.183 mg/m<sup>2</sup>. This value is probably a slight overestimation, since the porosity of the film is not taken into account. The swelling percentage (mass of water/dry mass of the film) was also calculated. The results in Table 1 show that the amount of water at both pH-values exceeds the amount of dry mass of cellulose. This fact suggests a highly swollen cellulose network. The measured water uptake value was found to be 4.39 mg/m<sup>2</sup>, and can be compared to unmodified low charged NFC film, where the value was 4.6 mg/m<sup>2</sup> (Aulin et al. 2009). However, due to the lower dry mass of the cationic NFC film, the swelling percentage is much higher, 137% compared to 24% for unmodified NFC. This is due to both higher charge and thinner fibrils leading to higher amount of accessible hydroxyl groups of the cationic nanofibril film. Although water can penetrate into the amorphous parts of the fibrils, the cellulose I crystalline parts are inaccessible for water. The dominating reasons for the water uptake are the charges, and the very high surface area of the network.

At a lower pH the same cationic film has higher water uptake value, which is explained by the higher

**Table 1** Sauerbrey mass of adsorbed water, and swelling percentage of cationic cellulose nanofibril films at different pH and electrolyte concentrations

Surface	Adsorbed water mass (mg/m <sup>2</sup> )	Swelling (%)
pH 8.0	4.39	137
pH 4.5	9.68	303
1 mM NaCl (pH 4.5)	9.98	nd
10 mM NaCl (pH 4.5)	8.61	nd
100 mM NaCl (pH 4.5)	7.78	nd

nd Not determined

net positive charge of the fibrils (see also Fig. 1). The carboxyl groups present within the cellulose chains are partly protonated at pH 4.5 and consequently they do not significantly affect the overall charge of the fibrils. The water uptake is higher when the network is more charged, and consequently the swelling percentage for film at pH 4.5 is very high, 303%.

Surprisingly, the water uptake was found to be insensitive to changes in electrolyte concentration at pH 8.0. An increase in NaCl concentration introduces a decrease in  $\Delta f$  comparable to the bulk effect, i.e. the change in frequency due changes in density and viscosity of the solvent as the electrolyte concentration is increased. The  $\Delta f$  for cationic NFC film on silica was  $-2$  Hz at 10 mM NaCl and  $-8$  Hz at 100 mM NaCl and for bare silica substrate the corresponding values were  $-1.8$  and  $-9$  Hz respectively. The energy dissipation curves show an increase in the dissipation for cationic NFC films at pH 8 while the buffer was added. This can be explained by the loosening of the NFC network upon addition of a buffer. However, a further increase in electrolyte concentration does not affect the dissipation values.

At pH 4.5, however, the film was sensitive to changes in electrolyte concentration as expected from simple electrostatic charge considerations. An addition of 0.1 mM NaCl does not significantly affect the swelling of the film. However an addition of 1 mM NaCl caused a small de-swelling of the NFC film, the frequency increased 5 Hz and the dissipation decreased  $3 \times 10^{-6}$ . Further addition of 10 and 100 mM NaCl caused further de-swelling of the NFC film (Lower graph in Fig. 7).

The difference between the electrostatic swelling behaviour at the two studied pHs may be understood in terms of electrostatic cross-linking. The anionic exchange capacity of the cationic NFC is 28  $\mu\text{eq/g}$  and the cationic exchange capacity of the cationic NFC is 354  $\mu\text{eq/g}$ . Hence, it would not be expected that the large difference in swelling at pH 8 compared to pH 4.5 would be explained solely by the net charge of the swollen film. Instead, it is suggested that there is an effect of electrostatic crosslinking between the carboxyl groups and the tertiary amino groups resulting in a stiffening of the gel network. This also readily explains why there is such a small effect of electrolyte addition at pH 8, where ionic cross-linking

is extensive. An increased electrolyte concentration is expected to decrease swelling, but the extent of electrostatic crosslinking is expected to be decreased with an increased ionic strength, so apparently the two effects are cancelling out each other at pH 8.

## Conclusions

Cationization prior to disintegration facilitated the production of extraordinary thin cationic cellulose I nanofibrils corresponding to elementary fibrils of cellulose. AFM measurements were conducted both in water and in air in order to characterize cationic NanoFibrillar Cellulose in its natural environment. For the first time the fibril size of never dried NFC was determined in aqueous media and the aggregation upon drying was discussed. Additionally cryo-TEM was used to confirm the small size of the fibrils, 2.6–3.5 nm, observed in the air state by AFM. A hypothesis was proposed that the cationic modification in addition to facilitate very effective fibrillation also partly dissolves the outer layer of the fibrils giving rise to fibrils having a diffuse highly swollen outer layer in aqueous media. The chemical composition and supramolecular structure of the cationic NFC was verified by XPS and Raman microspectroscopy. The response to pH and electrolyte changes of cationic NFC films was studied using QCM-D. Due to the amphoteric nature of the cationized NFC, the swelling was pH dependent. At all studied pHs the ultrathin NFC film swelled considerably. Yet at pH 8 the amount of bound water was remarkably insensitive to changes in electrolyte concentration, while the film behaved as a swollen polyelectrolyte gel at pH 4 and expelled water upon increasing the electrolyte concentration. This behaviour was suggested to be due to ionic cross-linking of the swollen film making it substantially stiffer at pH 8.

**Acknowledgments** This work has been performed as a part of “Design Cell” project in the Wood Wisdom.net. National Technology Agency of Finland, UPM Kymmene Corporation, Metso Oyj and Kemira Oyj is acknowledged for financial support. AO wishes to express her gratitude to Dr. Eero Kontturi for his help and inspiring scientific discussions. The experimental assistance of Marja Kärkkäinen is gratefully acknowledged. Joanna Hornatowska, Innventia, is acknowledged for here assistance in determining the size distribution in AFM-images.



## References

- Ahola S, Salmi J, Johansson LS, Laine J, Österberg M (2008a) Model films from native cellulose nanofibrils. Preparation, swelling, and surface interactions. *Biomacromolecules* 9:1273–1282
- Ahola S, Österberg M, Laine J (2008b) Cellulose nanofibrils-adsorption with poly(amideamine) epichlorohydrin studied by QCM-D and application as a paper strength additive. *Cellulose* 15:303–314
- Aulin C, Ahola S, Josefsson P, Nishino T, Hirose Y, Österberg M, Wågberg L (2009) Nanoscale cellulose films with different crystallinities and mesostructures; their surface properties and interaction with water. *Langmuir* 25:7675–7685
- Aulin C, Johansson E, Wågberg L, Lindström T (2010) Self-organized films from Cellulose I nanofibrils using the layer-by-layer technique. *Biomacromolecules* 11:872–882
- Baker AA, Helbert W, Sugiyama J, Miles MJ (1997) High-resolution atomic force microscopy of native valonia cellulose I microcrystals. *J Struct Biol* 119:129–138
- Bardage S, Donaldson L, Tokoh T, Daniel G (2004) Ultrastructure of the cell wall of unbeaten Norway spruce pulp fibre surfaces. *Nord Pulp Pap Res J* 19:448–452
- Beamson G, Briggs D (1992) High Resolution XPS of organic polymers. The Scienta ESCA300 Database. Wiley, Chichester
- Decher G, Schlenoff JB (2003) Multilayer Thin Films: Sequential assembly of nanocomposite Materials. Wiley-VCH, Weinheim
- Ding S-Y, Himmel ME (2006) The maize primary cell wall microfibril: a new model derived from direct visualization. *J Agric Food Chem* 54:597–606
- Dufresne A, Dupeyre D, Paillet M (2003) Lignocellulosic flour-reinforced poly(hydroxybutyrate-co-valerate) composites. *J Appl Polym Sci* 87:1302–1315
- Eichhorn SJ, Dufresne A, Aranguren M, Marcovich NE, Capadona JR, Rowan SJ, Weder C, Thielemans W, Roman M, Renneckar S, Gindl W, Veigel S, Keckes J, Yano H, Abe K, Nogi M, Nakagaito AN, Mangalam A, Simonsen J, Benight AS, Bismarck A, Berglund LA, Peijs T (2010) Review: current international research into cellulose nanofibres and nanocomposites. *J Mater Sci* 45:1–33
- Eronen P, Österberg M, Jääskeläinen A-S (2009) Effect of alkaline treatment on cellulose supramolecular structure studied with combined confocal Raman spectroscopy and atomic force microscopy. *Cellulose* 16:167–178
- Fahlen J, Salmen L (2003) Cross-sectional structure of the secondary wall of wood fibers as affected by processing. *J Mater Sci* 38:119–126
- Fält S, Wågberg L, Vesterlind EL (2003) Swelling of model films of cellulose having different charge densities and comparison to the swelling behavior of corresponding fibers. *Langmuir* 19:7895–7903
- Flory JP (1953) Principles of Polymer Chemistry. Cornell University Press, Ithaca
- Gilbert P, Moore LE (2005) Cationic antiseptics: diversity of action under a common epithet. *J Appl Microbiol* 99:703–715
- Gross AS, Chu J-W (2010) On the molecular origins of biomass recalcitrance: the interaction network and solvation structures of cellulose microfibrils. *J Phys Chem B* 114:13333–13341
- Hult EL, Larsson PT, Iversen T (2001) Cellulose fibril aggregation—an inherent property of kraft pulps. *Polymer* 42:3309–3314
- Iwamoto S, Abe K, Yano H (2008) The Effect of Hemicelluloses on wood pulp nanofibrillation and nanofiber network characteristics. *Biomacromolecules* 9:1022–1026
- Iwamoto S, Kai WH, Isogai A, Iwata T (2009) Elastic modulus of single cellulose microfibrils from tunicate measured by atomic force microscopy. *Biomacromolecules* 10:2571–2576
- Jakob HF, Fengel D, Tschegg SE, Fratzl P (1995) The elementary cellulose fibril in picea abies: comparison of transmission electron microscopy, small-angle X-ray scattering, and wide-angle X-ray scattering results. *Macromolecules* 28:8782–8787
- Johannsmann D, Mathauer K, Wegner G, Knoll W (1992) Viscoelastic properties of thin films probed with quartz-crystal resonator. *Phys Rev B* 46:7808–7815
- Johansson L-S, Campbell JM (2004) Reproducible XPS on biopolymers: cellulose studies. *Surf Interface Anal* 36:1018–1022
- Johansson L-S, Campbell JM, Kaljonen K, Kleen M, Buchert J (2004) On surface distributions in natural cellulosic fibres. *Surf Interface Anal* 36:706–710
- Johnson RK, Zink-Sharp A, Renneckar SH, Glasser WG (2009) A new bio-based nanocomposite: fibrillated TEMPO-oxidized celluloses in hydroxypropylcellulose matrix. *Cellulose* 16:227–238
- Katz K, Beatson RP, Scallan AM (1984) The determination of strong and weak acidic groups in sulphite pulps. *Svensk Papperstidning* 87(6):R48–R53
- Kondo T (1997) The relationship between intramolecular hydrogen bonds and certain physical properties of regioselectively substituted cellulose derivatives. *J Polym Sci Part B Polym Phys* 35:717–723
- Kontturi E, Tammelin T, Österberg M (2006) Cellulose-model films and the fundamental approach. *Chem Soc Rev* 35:1287–1304
- Li Q, Renneckar S (2009) Molecularly thin nanoparticles from cellulose: isolation of sub-microfibrillar structures. *Cellulose* 16:1025–1032
- Meshitsuka G, Isogai A (1996) Chemical structures of cellulose hemicellulose and lignin. In: Hon DN-S (ed) Chemical modification of lignocellulosic materials. Marcel dekker, New York, pp 11–33
- Mwaikambo LY, Ansell MP (2001) The determination of porosity and cellulose content of plant fibers by density methods. *J Mater Sci Lett* 20:2095–2096
- Naderi A, Claesson PM (2006) Adsorption properties of polyelectrolyte-surfactant complexes on hydrophobic surfaces studied by QCM-D. *Langmuir* 22:7639–7645
- Pääkkö M, Ankerfors M, Kosonen H, Nykänen A, Ahola S, Österberg M, Ruokolainen J, Laine J, Larsson PT, Ikkala O, Lindström T (2007) Enzymatic hydrolysis combined with mechanical shearing and high-pressure homogenization for nanoscale cellulose fibrils and strong gels. *Biomacromolecules* 8:1934–1941

- Phillips DL, Xing J, Liu H, Chong CK, Corke H (1999) Raman spectroscopic determination of the degree of cationic modification in waxy maize starches. *Anal Letters* 32:3049–3058
- Pigorsch E (2009) Spectroscopic characterization of cationic quarternary ammonium starches. *Starch* 61:129–138
- Saito T, Nishiyama Y, Putaux J-L, Vignon M (2006) Homogeneous suspensions of individualized microfibrils from TEMPO-catalyzed oxidation of native cellulose. *Biomacromolecules* 7:1687–1691
- Saito T, Kimura S, Nishiyama Y, Isogai A (2007) Cellulose nanofibers prepared by TEMPO-mediated oxidation of native cellulose. *Biomacromolecules* 8:2485–2491
- Sakurada I, Nukushina Y, Ito T (1962) Experimental determination of the elastic modulus of crystalline regions in oriented polymers. *J Polym Sci* 57:651–660
- Salmi J, Nypelö T, Österberg M, Laine J (2009) Layer Structure formed by silica nanoparticles and cellulose nanofibril with cationic polyacrylamide (C-PAM) on cellulose surface and their influence on interactions. *Bioresources* 4:602–625
- Sauerbrey G (1959) The use of quartz oscillators for weighing thin layers and for microweighing. *Z Phys* 155:206–222
- Siró I, Plackett D (2010) Microfibrillated cellulose and new nanocomposite materials: a review. *Cellulose* 17:459–495
- Sugiyama J, Vuong R, Chanzy H (1991) Electron diffraction study on the two crystalline phases occurring in native cellulose from an algal cell wall. *Macromolecules* 24:4168–4175
- Taipale T, Österberg M, Nykänen A, Ruokolainen J, Laine J (2010) Effect of microfibrillated cellulose and fines on the drainage of kraft pulp suspension and paper strength. *Cellulose* 17:1005–1020
- Tammelin T, Saarinen T, Österberg M, Laine J (2006) Preparation of Langmuir/Blodgett-cellulose surfaces by using horizontal dipping procedure. Application for polyelectrolyte adsorption studies performed with QCM-D. *Cellulose* 13:519–535
- Vietor RJ, Newman RH, Ha MA, Apperley DC, Jarvis MC (2002) Conformational features of crystal-surface cellulose from higher plants. *Plant J* 30:721–731
- Virtanen T, Maunu SL, Tamminen T, Hortling B, Liitiä T (2008) Changes in fiber ultrastructure during various kraft pulping conditions evaluated by <sup>13</sup>C CPMAS NMR spectroscopy. *Carbohydr Polym* 73:156–163
- Wågberg L, Winter L, Ödberg L, Lindström T (1987) On the charge stoichiometry upon adsorption of a cationic polyelectrolyte on cellulosic materials. *Colloids Surf* 27:163–173
- Wågberg L, Decher G, Norgren M, Lindström T, Ankerfors M, Axnäs K (2008) The build-up of polyelectrolyte multilayers of microfibrillated cellulose and cationic polyelectrolytes. *Langmuir* 24:784–795
- Wählby C, Erlandsson F, Nyberg K, Lindblad J, Zetterberg A, Bengtsson E (2001) Proceedings of 12th scandinavian conference on image analysis, Bergen, Norway
- Wang Y, Chen HY (2007) Carbon nanotubes: a promising standard for quantitative evaluation of AFM tip apex geometry. *Ultramicroscopy* 107:293–298
- Wang M, Olszewska A, Walther A, Malho J-M, Schacher FH, Ruokolainen J, Ankerfors M, Laine J, Berglund LA, Österberg M, Ikkala O (2011) Colloidal ionic self-assembly between anionic native cellulose nanofibrils and cationic lock copolymer micelles into biomimetic nanocomposites. *Biomacromolecules* 12:2074–2081
- Wiley JH, Atalla RH (1987) Band assignments in the Raman spectra of celluloses. *Carbohydrates Res* 160:113–129
- Yano H, Sugiyama J, Nakagaito AN, Nogi M, Matsuura T, Kikita M, Handa K (2005) Optically transparent composites reinforced with networks of bacterial nanofibers. *Adv Mater* 17:153–155
- Zimmermann T, Pöhler E, Geiger T (2004) Cellulose fibrils for polymer reinforcement. *Adv Eng Mater* 6:754–761